Surface modification of microporous PVDF membranes by ATRP

Nripen Singh [a,c], Scott M. Husson [a,c,*], Bogdan Zdyrko [b,c], Igor Luzinov [b,c]

[a] *Department of Chemical and Biomolecular Engineering, Clemson University, 127 Earle Hall, Clemson, SC 29634, USA*
[b] *School of Materials Science and Engineering, Clemson University, Clemson, SC 29634, USA*
[c] *Center for Advanced Engineering Fibers and Films, Clemson University, Clemson, SC, USA*

Abstract

This contribution describes a methodology to convert commercially available, microporous membranes into ion-exchange membranes using primary anchoring polymer (mono)layers and graft polymerization from the surfaces of the membranes. Atom transfer radical polymerization (ATRP) was used to modify the membranes with pyridinium exchange groups. Polymerization time was used as the independent variable to manipulate the amount of grafted poly(2-vinylpyridine) on the membrane surface. Results indicate that by changing polymerization time, it is possible to tune the ion-exchange capacity and the average pore size in rational ways. Equally important, membranes with initially broad pore-size distributions had narrower pore-size distributions following polymerization. A polymerization time of 24 h reduced the pore-diameter polydispersity (PDP) from 2.05 to 1.44. A polymerization time of 8 h resulted in a static ion-exchange capacity of 7.32×10^{-2} mmol/g (7.32×10^{-2} meq/g) of dry membrane.
© 2005 Elsevier B.V. All rights reserved.

Keywords: Atom transfer radical polymerization; Capacity; Graft polymerization; Pore-size distribution

1. Introduction

Membrane chromatography is a unit operation that is suited well for bioseparation applications involving large proteins and macromolecules, such as plasmid DNA [1–5]. The advantages of membrane chromatography over traditional packed-bed chromatography include improved mass-transfer efficiency, lower pressure drop, more efficient ligand utilization, easier scalability, and lower cost [6]. Because solute is transported to the membrane binding sites primarily by convection, rather than diffusion, processing rates can be orders of magnitude higher for membrane chromatography systems [7,8]. In addition, membrane chromatography modules have higher dynamic binding capacities than traditional packed-bed systems for large biomolecules (e.g., plasmid DNA) that have mega-Dalton molecular weight values. For example, Endres et al. [5] found that dynamic binding capacity and flow rate for pDNA on Mustang Q ion-exchange membranes were 20–25 times greater and 55–550 times greater, respectively, than values observed for beads. Teeters et al. [9] also reported a maximum binding capacity for pDNA on Mustang Q ion-exchange membranes that were an order of magnitude higher than conventional porous beads.

In order to exploit the advantages of membrane chromatography for large molecule separations, it is important to tune the physical and chemical properties of the membrane surface, since these play important roles in determining its separation characteristics, including efficiency and productivity. For example, commercially available microporous membranes contain a relatively broad distribution of pore sizes. The broad pore-size distribution leads to inefficient utilization of the membrane because pores of different sizes have different solute residence times and capacities; these factors, in turn, result in a broad distribution of breakthrough curves for individual pores [10]. For membranes as a whole, composite breakthrough curves broaden as pore-size distributions broaden. Also, important is the size of the pores in relation to the solute size.

The previous example illustrates how membrane physical properties influence separation. Membrane surface chemistry also impacts separation performance. For example, binding amino acids, proteins, dyes, ion-exchange groups, and metal affinity ligands covalently to the surfaces of polymeric membranes transforms them into pseudo-biospecific affinity membranes for the purification of proteins. In fact, membrane surface modification is thought to be equally important to the membrane industry as membrane material and process development. Therefore, there is significant interest in developing surface treatment methods to modify base membrane properties post synthesis. Graft modification strategies have been used to tailor membranes for bioseparation applications, and excellent, comprehensive reviews are available for affinity membrane [11] adsorptive membrane [3] and ion-exchange membrane [12] applications in biotechnology.

The (photo)chemical means used to incorporate affinity or ion-exchange groups into a porous membrane depends on the chemistry of the membrane surface. For relatively chemically inert membranes, e.g., polyethylene (PE), the surface must first be treated to produce reactive sites for further surface modification. A common approach uses e-beam or γ-ray irradiation to graft reactive poly(glycidyl methacrylate) (PGMA) to the membrane surface [13–17]. The epoxy groups of the grafted PGMA serve as reaction sites to incorporate affinity ligands, amino acid groups [13,14,17] metal-chelating agents [17] for binding histidine-containing peptides and proteins [15], and ion-exchange groups [12,16,17]. Ultraviolet grafting of polyacrylic acid (PAA) has also been used for attaching amino acids on PE membranes [18].

Cellulose-based and specialty co-polymer membranes provide the requisite reaction sites for surface modification without pretreatment. For example, Guo and Ruckenstein [19,20] have described affinity modification of cellulose membranes. Cattoli and Sarti [21] modified a microporous cellulose membrane with amylose, and used these affinity membranes in a chromatography module to purify proteins containing the maltose-binding protein (MBP) domain from crude cell lysate. Luo et al. [22] reacted L-histidine onto a poly(glycidyl-co-ethylene dimethacrylate) polymer film and used it to purify IgG from human serum.

Finally, for membranes made of polymers such as PC, PET, polysulfone (PS), polyamides, etc., the functional end groups of the polymer chains provide reaction sites for surface modification. While Klein [11] has shown that the end group concentration is high enough to produce membranes with capacities nearing those of synthetic chromatography beads, opportunities exist for increasing or amplifying the number of reactive surface sites from the chain ends.

Reaction site amplification typically involves grafting functionalized polymers to or graft polymerization from the chain ends. The functional groups on the graft polymers serve as additional reactive sites to attach ligand groups. For example, Klein et al. [23] modified microporous PS hollow fibers by anchoring hydroxyethyl cellulose (HEC) polymers covalently to terminal phenol groups. Further functionalization of

the HEC chains with recombinant protein A resulted in affinity membranes for IgG. Beeskow et al. [24] used HEC to modify microporous polyamide membranes. Immobilizing HEC to the polyamide membranes reduced non-specific protein binding, while simultaneously increasing binding sites for affinity ligands. Finally, UV photografting has been used extensively by Belfort and co-workers (see, e.g., Refs. [25,26]) to modify poly(ether sulfone) nanofiltration membranes and by Yang and Yang [27] to modify PET nucleopore membranes. This approach modifies the exposed membrane surfaces, as opposed to modifying the membrane bulk.

This contribution describes the use of atom transfer radical polymerization (ATRP) and reactive primary polymer (mono)layers to functionalize commercially available poly(vinylidenefluoride) microporous membranes with weak ion-exchange groups. ATRP was used to grow poly(2-vinylpyridine) from a primary anchoring polymer monolayer containing epoxide functional groups that had been anchored to the membrane pore surfaces. As a controllable chain growth technique, ATRP allows design and manipulation of the chain MW [28], which, in turn, should allow controlled manipulation of membrane pore size. Furthermore, we have shown that ATRP produces more uniform surfaces than conventional radical polymerization [29]. ATRP reaction conditions are flexible; therefore, we used solvents that maintained membrane integrity. These features are important for membrane modifications for bioseparations since membrane materials impose limitations on solvent selection for modification reactions, and since control of graft polymer molecular weight is important to avoid pore filling.

A goal of this work was to examine whether ATRP could be used to simultaneously change the surface functionality, pore size, and pore-size distribution in rational ways. Polymerization time was used as the independent variable to manipulate the amount of grafted poly(2-vinylpyridine) on the membrane surface. Results are presented that show that a membrane with an initially broad pore-size distribution had a narrower pore-size distribution following polymerization. This result is an important advantage to avoid inefficient membrane utilization caused by premature solute breakthrough. Additional results are presented that demonstrate how changing polymerization time allows one to tune the ion-exchange capacity and the average pore size of the membranes.

2. Experimental materials and methods

2.1. Materials

Hydrophilic polyvinylidenedifluoride (PVDF) membranes (Millipore Durapore®, 0.45 μm, 25 mm diameter, 125 μm thickness) were purchased from Millipore Inc. All chemicals were purchased from Aldrich and used as received, unless noted otherwise; they were glycidyl methacrylate

(95%), azobisisobutyronitrile (98%), bromoacetic acid (99%), 2-vinylpyridine (97%), copper(I) bromide (99.999%), 1,4,8,11-tetraazacyclotetradecane (Me$_4$Cyclam, 98%), hydrochloric acid (37%, aqueous). Solvents were purchased from Aldrich as ACS reagent grade; they were ethyl alcohol (99.5%), methanol (99%), anhydrous toluene (99.8%), acetonitrile (>99.9%) and methyl ethyl ketone (MEK, 99.6%). Reported percentages are in wt%. 2-Vinylpyridine was purified with vacuum distillation at 33.3306×10^2 Pa (25 mmHg) before use to remove the inhibitor (*p-t*-butyl catechol).

2.2. Preparing membranes for initiator functionalization

According to the Millipore patent [30], the hydrophilic PVDF membrane is modified with a poly(oxyethylene-co-oxypropylene) surfactant deposited from methanol solution. All membranes were washed in warm methanol to try to remove this surfactant. A Harrick plasma cleaner/sterilizer (model PRC-32G) was used to generate plasma at a middle RF level, and the membrane was plasma treated on one side for 3 min, flipped, and plasma treated on the second side for an additional 3 min. Pressure during plasma treatments was 0.1333224×10^2 Pa (0.1 Torr). The plasma-treated membrane was rinsed three times for 10 min each in MEK and dried with a nitrogen stream before grafting the anchoring epoxide layer.

2.3. Grafting the primary epoxide layer

Poly(glycidyl methacrylate) was used to form a reactive primary polymer layer [31–34]. A polymer with epoxy functionality was chosen because the reactions of the epoxy group are quite universal. It reacts with different functional groups (hydroxyl, amino, carboxyl, etc.) present, or that can be created on the surfaces of various membranes. Thus, the epoxy functionalities were used to anchor PGMA covalently to the plasma-treated membrane surface.

Glycidyl methacrylate was polymerized radically to give PGMA with $M_n = 84,000$ and PDI = 3.4 (GPC). Briefly, the polymerization was carried out in MEK at 60 °C. Azobisisobutyronitrile was used as an initiator. The polymer obtained was purified by multiple precipitations from the MEK solution by diethyl ether. Plasma-treated membranes were placed in a round bottom flask with 10 mL of 0.2 wt% PGMA solution in MEK. The flask was vacuum evacuated until the solution started to boil, and air was introduced back to the flask. The above treatment was repeated three times to ensure penetration of the PGMA solution into the membrane pores. The soaked membrane was dried with nitrogen and aged under a nitrogen atmosphere at 40 °C for 2 h. Subsequent rinsing (three times at 10 min) with pure MEK removed non-bonded PGMA from the membrane. To functionalize the membrane with ATRP initiator groups, the PGMA modified membrane was placed into a test tube with a crystal(s) (10–20 mg) of bromoacetic acid. The test tube was vacuum evacuated and placed in an oven at 90 °C for 1 h. Reaction

of vapor-phase bromoacetic acid with the remaining epoxide groups of PGMA produced tethered bromoacetate groups capable to initiate ATRP [32,33]. After treatment, the membrane was rinsed three times in MEK for 10 min each and dried with a nitrogen stream.

2.4. Surface graft polymerization of poly(2-vinylpyridine)

Polymerization was carried out in acetonitrile as the solvent and using 2-vinylpyridine as the monomer. This step used an organometallic catalyst comprising Cu(I)Br and ligand 1,4,8,11-tetraazacyclotetradecane (Me$_4$Cyclam) with a molar ratio of 1:2. The concentration of 2-vinylpyridine was 2 M, and the catalyst concentration was 2 mM based on Cu(I). Both solvent and monomer were degassed using three freeze-pump-thaw cycles with vacuum evacuation and N$_2$ purging. The solution flask was isolated under an N$_2$ blanket from the de-oxygenation line and transferred to an oxygen-free glove box. All polymerization steps were carried out at room temperature in an oxygen-free glove box to avoid catalyst oxidation. To begin polymerization, initiator-functionalized membranes were placed in 10 mL of the monomer/catalyst solution. After polymerization for up to 24 h, the membranes were removed from the polymerization system, washed in acetonitrile using an ultrasonic bath for 10 s, rinsed with acetonitrile, ethanol and deionized water, and dried in a stream of nitrogen.

Polymerization reaction time was the independent variable in this study. Dependent variables were membrane ion-exchange capacity, surface and bulk average pore sizes, and pore-size distribution. Titration was used to measure ion-exchange capacity of the membranes, while FE SEM (with Image Pro Analysis) and nitrogen adsorption experiments were used to characterize the average pore sizes and pore-size distributions of each membrane.

Membrane surfaces were characterized by ATR-FTIR to elucidate the chemical properties of our modified membranes and scanning probe microscopy was used to follow morphological changes to the membrane surfaces. These measurements allowed us to examine the uniformity of the graft surfaces.

2.5. Attenuated total reflectance Fourier transform infrared spectroscopy (ATR-FTIR)

ATR-FTIR spectra were obtained for an unmodified control membrane; initiator-functionalized, PGMA-coated membrane; and poly(2-vinylpyridine) grafted membranes using a Thermo-Nicolet Magna 550 FTIR spectrometer equipped with a diamond, single bounce foundation series ATR accessory and a 50° angle of incidence. Each spectrum was obtained by cumulating 32 scans at a resolution of 4 cm^{-1}. Data were corrected using ATR correction and background correction functions of OMNIC ESP software, Version 6.1a.

2.6. Field emission scanning electron microscope (FE SEM)

The morphologies of the membrane surfaces before and after modification were studied by field emission scanning electron microscopy (FE SEM) using a Hitachi FE SEM 47,000. Representative samples of the membranes were cut into 0.5 cm^2, attached with carbon tape to aluminum stabs, and shadowed with platinum prior to the SEM measurements. The SEM measurements were performed at an accelerating voltage of 5 kV to evaluate the extent of the surface porosity and microstructure.

SEM images were taken of the porous surfaces and analyzed with the digital imaging technique (Image-Pro PLUS Analysis software) to estimate the surface pore sizes and to generate pore-size distributions for samples prepared at different polymerization times. For each sample, data were used to calculate the average surface pore diameter and pore-diameter polydispersity.

2.7. Atomic force microscopy (AFM)

Topographical and phase images and roughness values of the poly(2-vinylpyridine) functionalized membrane surfaces were obtained using a BioScope AFM (Veeco) with Nanoscope IIIa controller. Both tapping and phase-imaging modes were used to characterize the film surface in ambient air. The root-mean-square roughness values of the samples were evaluated from AFM images in the tapping mode. The height (topography) and phase images were both captured using a frequency of 1.0 Hz and 256 scan lines per image. Surface roughness was determined using the NanoScope Software Version 5.12 root-mean-square (RMS) roughness calculation.

2.8. Nitrogen adsorption

The bulk membrane pore sizes, pore volumes and pore areas were determined by static volumetric measurements of nitrogen adsorption. A Micrometrics 2020 instrument was used to measure nitrogen adsorption isotherms at $-196\,°C$ between pressures of 5.06625×10^{-2} and 1.01325×10^5 Pa (5×10^{-7} and 1 atm). All samples were outgassed at 125 °C for 6 h prior to each adsorption experiment to remove contaminants adsorbed by exposure to the atmosphere. The same instrument was used to measure adsorption and desorption isotherms on selected samples. Evaluation of the adsorption and desorption branches of these isotherms and the hysteresis between them reveals information about the membrane pore characteristics.

2.9. Ion-exchange capacity measurements

Ion-exchange capacity measurements were done potentiometrically using a Mettler Toledo (DG-I I I-SG) titrator. Titration was done using standardized 0.01 M HCl solution to estimate of the number of pyridine groups per unit mass attached to the membrane surfaces. Standardization of the HCl solution was done by titration against 1 M NaOH that had been standardized by titration with potassium hydrogen phthalate solution, as outlined by Hoover et al. [35]. A titration curve was prepared by adding incremental doses of HCl solution to the beaker containing membrane cut into approximately 1 cm × 0.5 cm pieces. Stirring was done continuously. After each dose of acid, the system was allowed to equilibrate, and the pH was measured with a 3 M KCl (0–14) pH electrode. Ion-exchange capacities of the membranes were calculated in milliequivalents per gram of dry membrane.

3. Results and discussion

3.1. Characterization of chemical and physical surface properties

Characterization of the chemical and physical properties of the membranes surfaces was done by ATR-FTIR, AFM, FE SEM, nitrogen adsorption measurements and image analysis.

Fig. 1 presents typical ATR-FTIR spectra for an unmodified control membrane (spectrum 1a), an initiator-functionalized membrane (spectrum 1b), and a poly(2-vinylpyridine) functionalized membrane (spectrum 1c) following 24 h of polymerization. According to the manufacturer, the peak at 1732 cm^{-1} in the unmodified membrane is associated with the carbonyl stretch of polyacrylate groups that are introduced to the PVDF membranes to make them hydrophilic. Unfortunately, this peak interferes with and overwhelms the peak signal for the carbonyl stretch of the initiator. Nevertheless, the appearance of C=N stretching modes in the pyridine ring at 1593 and 1569 cm^{-1} and a C=C stretching mode in the pyridine ring at 1475 cm^{-1} (spectrum 1c) support the successful grafting of poly(2-vinylpyridine) to the membrane surface.
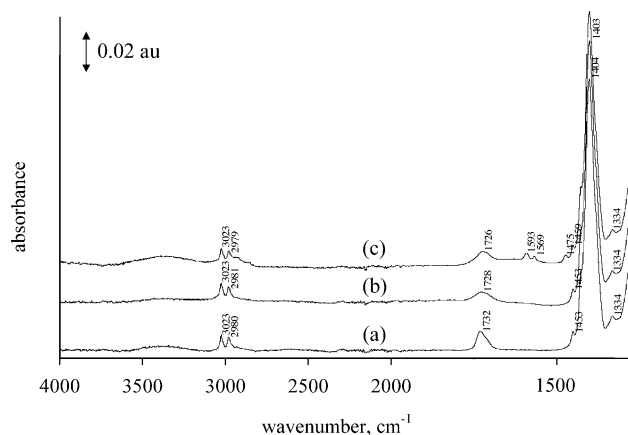
Fig. 1. ATR-FTIR spectra for (a) unmodified control membrane; (b) initiator-functionalized, PGMA-coated membrane; (c) poly(2-vinyl-pyridine) grafted membrane after 24 h of polymerization.
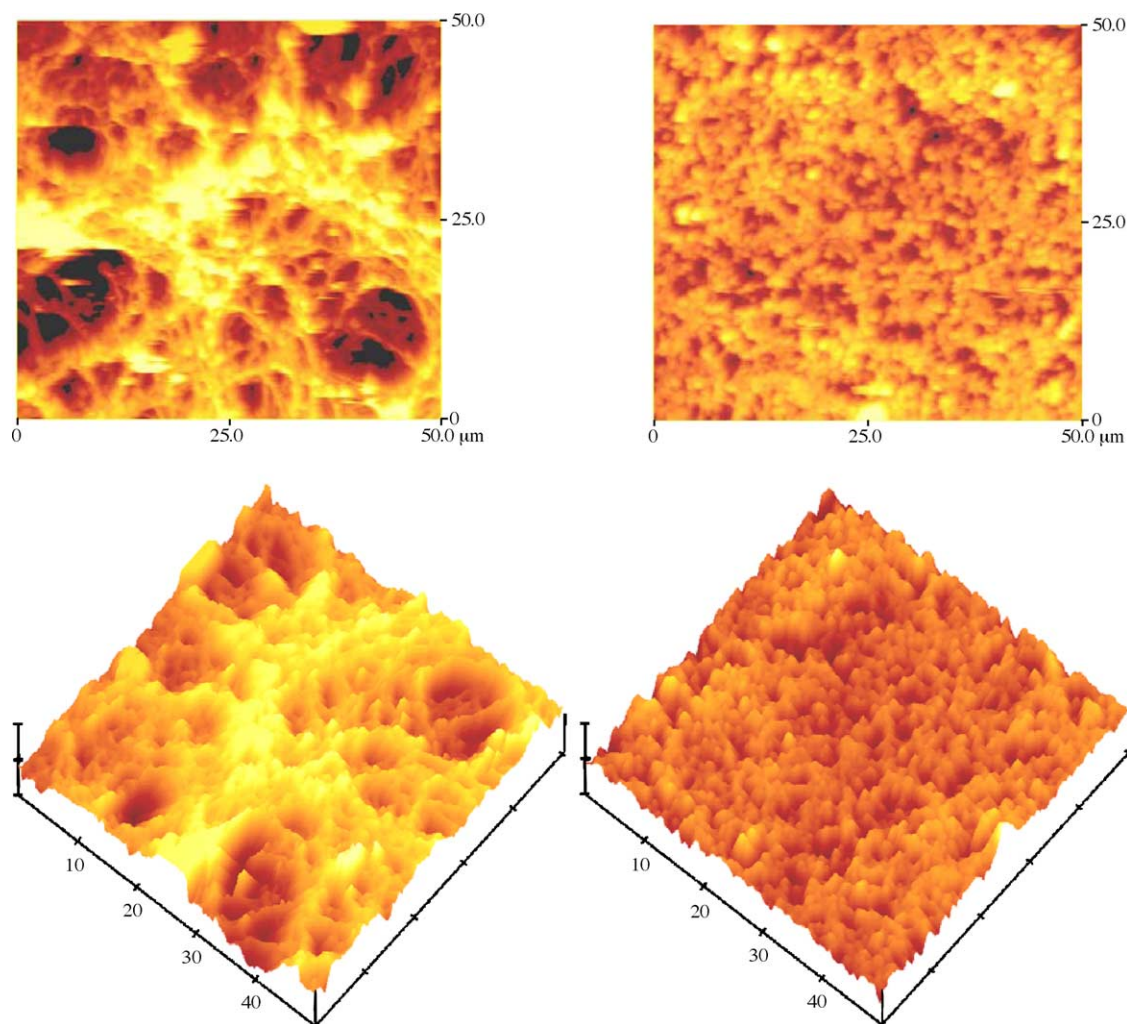
Fig. 2. AFM phase and topographical images (50 μm × 50 μm lateral area) showing the morphology of the surfaces. The *z*-axis scale is 4500 nm. RMS roughness values are 1.186 μm and 352 nm for the unmodified and modified membranes, respectively.

Atomic force microscopy was performed to examine the surface morphology and to measure roughness values for unmodified and poly(2-vinylpyridine)-modified membrane surfaces. Fig. 2 shows typical phase and topographic scans of the unmodified and polymer-modified membrane surfaces. Each scan represents a 50 μm × 50 μm lateral area. Fig. 2 reveals that the polymer-modified surface was smooth and uniform compared to the control membrane surface. The modified membrane surface had a root-mean-square roughness, RMS = 352 nm; the control surface had a root-mean-square roughness, RMS = 1.186 μm. This result is consistent with other published works that report that surface-confined polymerization can significantly change surface morphology [36] and smoothen rough surfaces [36–38]. Freger et al. [37], for example, reported decreased surface roughness values from 93 to 30 nm for Dow Filmtec reverse osmosis membranes following graft polymerization of polyethylene glycol methacrylate and sulfopropyl methacrylate. Tanaguchi et al. [38] reported decreased vertical roughness values on 12 of

17 samples following UV graft polymerization of *N*-vinyl-2-pyrrolidinone on poly(ether sulfone) membranes.

3.2. Determination of specific surface areas and pore characteristics from nitrogen adsorption isotherms

The method of Brunauer–Emmett–Teller (BET) was employed to determine surface area based on a model of adsorption that incorporates multilayer coverage. The Barrett–Joyner–Halenda (BJH) method was applied to the isotherms to measure the pore sizes and pore-size distribution using the Kelvin model of pore filling. Nitrogen was admitted into the membrane chamber in controlled increments. After each dose of adsorptive, the pressure was allowed to equilibrate and the volume of nitrogen adsorbed was calculated. A plot of the gas volume adsorbed versus pressure (at constant temperature) defines an adsorption isotherm, from which the volume of gas required to form a monolayer over the external surface and its pores was determined. Knowing the value for

Table 1
BET surface areas and BJH desorption average pore width of the PVDF membranes for untreated and treated membranes prepared using different polymerization times

Polymerization time (h)	BET surface area (m^2/g)	BJH desorption average pore width (Å)
0	2.21	84.6
1	2.49	98.4
2	2.59	106.0
8	2.71	111.8

the area covered by each adsorbed molecule to be 16.2 Å^2 [39], the surface area was calculated for each sample.

Table 1 summarizes the BET surface area data. These data confirm that these porous membranes have relatively low specific areas that increase slightly from 2.21 to 2.71 m^2/g with increasing polymerization time. Surface area changes depend on two competing factors: loss of accessible surface area due to blocking of small pores and creation of surface area by growth of polymer chains that extend from the pore surfaces. The latter factor assumes that nitrogen molecules are able to penetrate in between chains and, in this case, appears to compensate for area loss due to pore blockage.

By extending this process to pressure conditions that condense the gas into the pores, pore sizes and the pore-size distribution can be evaluated. After reaching high enough pressures to ensure gas condensation, the adsorptive gas pressure is reduced incrementally, thereby evaporating the condensed gas from the system. Table 1 shows average bulk pore diameter values calculated using the BJH method; *average* diameters increased from 84.6 to 111.8 Å with increasing polymerization time. This result was unexpected. One contributing factor to this increase in average pore size may be the blockage of the smallest pores as a result of polymer growth. Additionally, under the conditions used for the adsorption experiments, only pore sizes in the mesopore range of 2–50 nm could be measured. We speculate, then that two additional processes may have contributed to the increase in average BJH pore diameter: the transformation of a large number of pores from the low end of the mesopore range into the micropore region, and transformation of macropores into large mesopores as a result of polymer growth within the pores.

All adsorption–desorption isotherms displayed Type H4 hysteresis loops, which are characteristic of narrow slit-like mesopores [39], and the degree of hysteresis increased as the polymerization time increased. One possible explanation of this result is that polymer growth may have partially occluded spherical pores. The resulting pore would have a restricted diameter at its entrance, and this ink-bottle type of morphology would lead to an increase in degree of hysteresis [40].

3.3. Surface morphologies of the modified PVDF membranes

Fig. 3(a–c) shows surface SEM images at a magnification of 1000× for the unmodified PVDF membrane; initiator-

functionalized, plasma-treated membrane; and the poly(2-vinylpyridine) functionalized membrane following 24 h polymerization. Fig. 3(d–f) shows the corresponding SEM images at a magnification of 2000×. The PVDF membrane exhibits a rich fibrous structure before the modification that appears to densify after polymerization. Figs. 3(c and f) shows that the membrane fibers have grown thicker and the pore sizes have become more uniform for the poly(2-vinylpyridine) functionalized membranes. Both the unmodified and modified membranes show a homogenous morphology in their cross-sections as well on the surfaces. The cross-sectional views of the modified membranes in Fig. 4 shows that the polymer was grafted on the membrane outer surface and also from the pore surfaces within the bulk of the membranes.

3.4. Determination of pore-size distribution by image analysis of SEM images

Image-Pro PLUS software was used to determine the membrane surface pore-size distributions and pore-diameter polydispersity values following polymerization for various times. By changing polymerization time, the average *surface* pore diameter decreased from 1.11 to 0.98 μm, corresponding to a polymer thickness of about 600 Å. Using similar conditions to grow poly(2-vinylpyridine) from self-assembled monolayer (SAM) surfaces, Li et al. [29] measured ellipsometric thicknesses of 105 ± 15 Å. To understand this apparent discrepancy, it is necessary to compare the surface initiator densities for SAM versus PGMA layers and the impact of initiator densities on subsequent polymer layer thicknesses. Liu et al. [33] have shown that for a 6 nm thick surface layer of PGMA, the surface density of initiator ($\sim$40 nm^{-2}) is an order of magnitude higher than that for a SAM layer on gold ($\sim$3 nm^{-2}). In that same paper, it was demonstrated that increasing the surface density of initiator from $\sim$3 to $\sim$40 nm^{-2} led to a six-fold increase in polystyrene layer thickness for the same polymerization time. Therefore, with a similar enhancement in layer thickness, one would anticipate a poly(2-vinylpyridine) layer thickness of $\sim$630 ± 90 Å, which is consistent with the average pore diameter decrease of 1200 Å.

Equally important, the pore-size distribution became narrower following polymerization. Fig. 5 shows the narrowing down of the pore-size distribution as more polymer is grafted on the membrane surfaces. By defining a pore-diameter polydispersity (PDP) as the weight-average diameter divided by the number-average diameter, the change in pore-size distribution was quantified (a PDP value of 1.0 means that all pores are equal in size). Initially, for unmodified membranes, PDP was 2.05; following polymerization for 24 h, it was reduced to 1.44. Table 2 shows the time-dependent trend in the PDP clearly showing that the pore diameters have become more uniform.

A control experiment was conducted that subjected an unmodified membrane to all steps of the process except the initiator functionalization. The purpose of this control experiment was to determine if the pore size properties of the
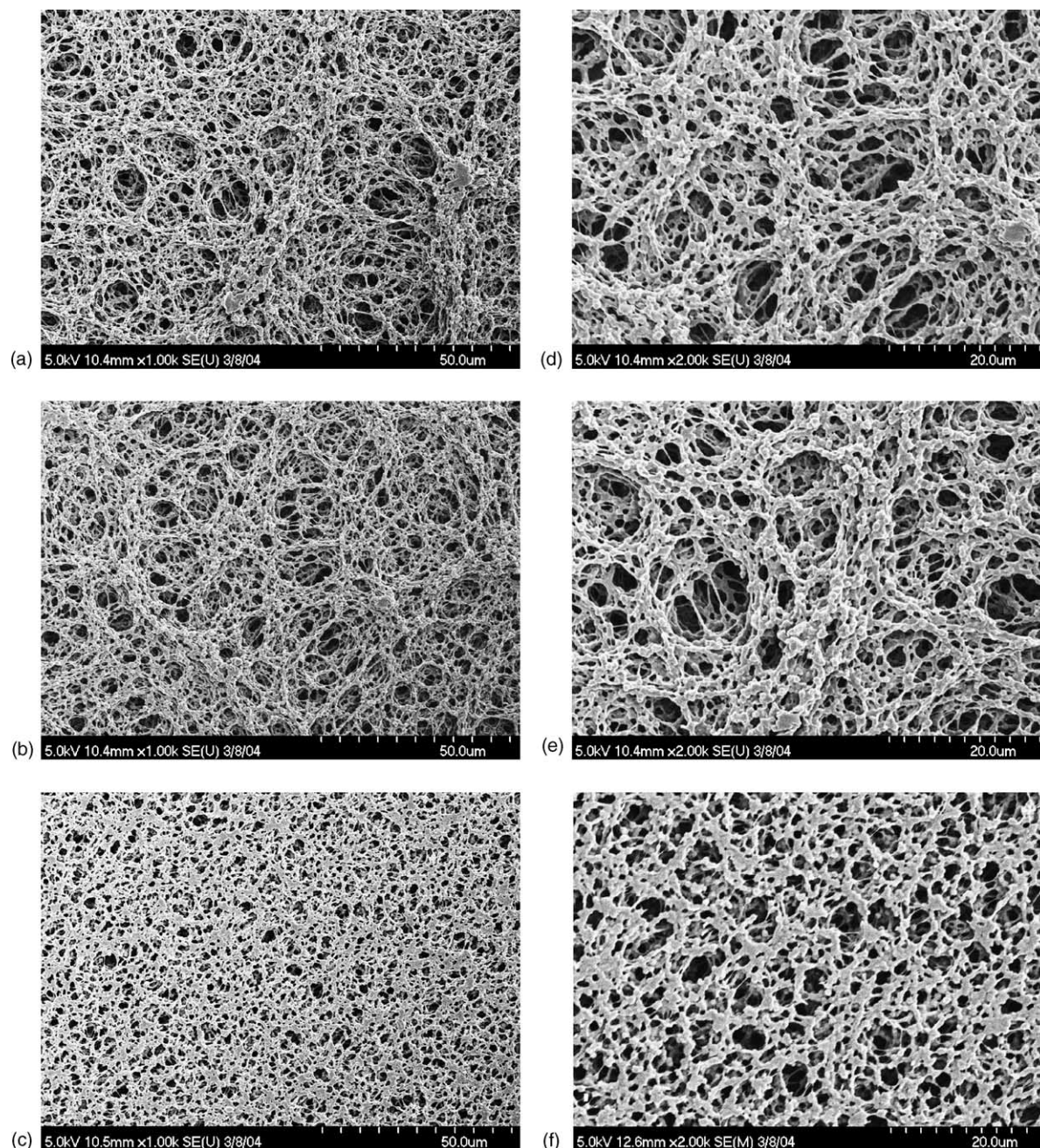
Fig. 3. Images (a–c): surface SEM micrographs of the unmodified PVDF membrane (a); initiator-functionalized, plasma-treated membrane (b); the poly(2-vinylpyridine) (c) functionalized membrane at a magnification of 1000×. Images (d–f): corresponding micrographs at a magnification of 2000×.

membrane changed as a result of chemical exposure in the absence of poly(2-vinylpyridine) growth. SEM image analysis showed the average surface pore diameter to be 1.09 μm and the PDP to be 1.95. Therefore, chemical exposure and PGMA grafting alone cannot account for the observed decreases in average pore diameter and PDP.

3.5. Ion-exchange capacity measurements

Ion-exchange capacities for the modified membranes were measured by generating titration curves of the pyridine groups on the membrane surfaces against 0.01 M HCl. Table 3 shows the increase in the static ion-exchange capacity of the membranes from 2.25×10^{-2} to 7.32×10^{-2} mmol/g (2.25×10^{-2} to 7.32×10^{-2} meq/g) with an increase in the polymerization time from 1 to 8 h. For ion exchange of small molecules, these values are low compared to commercially available ion-exchange membranes, which typically have capacities of 1–3 mmol/g (1–3 meq/g) [41].

ATRP is often described as a controlled radical polymerization because irreversible termination reactions that
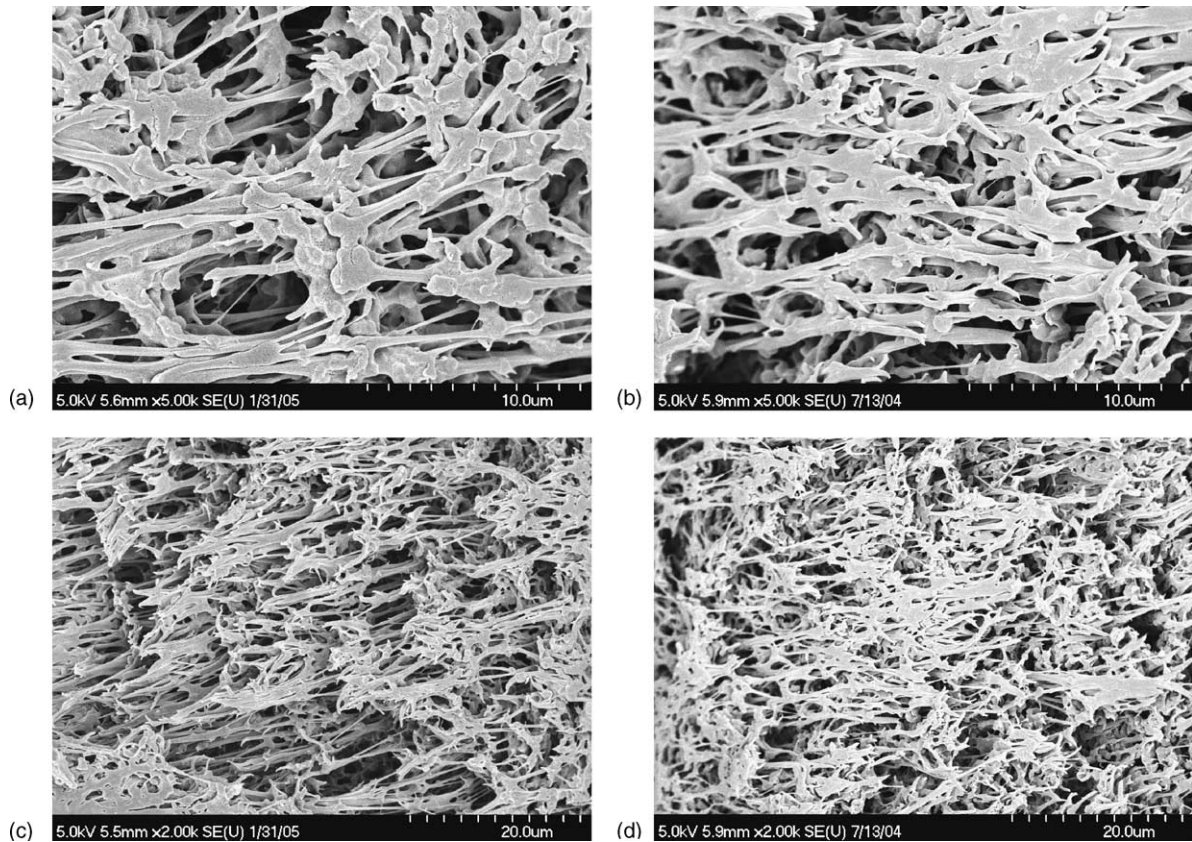
Fig. 4. Images (a–b): cross-sectional SEM micrographs of the unmodified PVDF membrane (a) and the poly(2-vinylpyridine) functionalized membrane (b) at a magnification of 5000×. Images (c–d): corresponding micrographs at a magnification of 2000×.
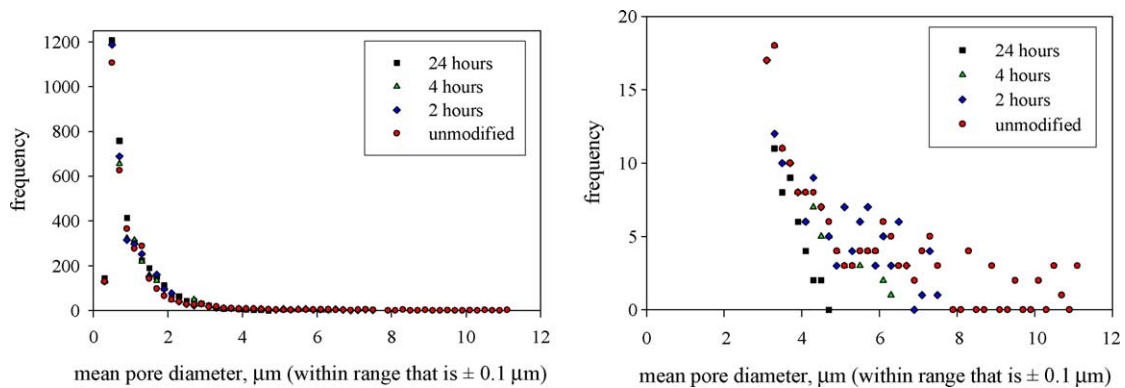
Fig. 5. Pore-size distribution of the unmodified PVDF membrane and the poly(2-vinylpyridine) functionalized membrane at different polymerization times. The figure on the right expands the frequency axis to illustrate the depletion of large pore structures.

Table 2
Number-average pore diameter and PDP for membranes prepared using different polymerization times

Polymerization time (h)	Number-average pore diameter (d_n) (μm)	PDP (d_w/d_n)
0	1.11	2.05
2	1.08	1.98
4	1.05	1.75
24	0.98	1.44

Table 3
Ion-exchange capacities (mmol/g (meq/g)) for membranes prepared using different polymerization times

Polymerization time (h)	Ion-exchange capacity ($\times 10^{-2}$ mmol/g ($\times 10^{-2}$ meq/g))
1	2.25
2	3.12
4	5.36
8	7.32

consume radicals are suppressed by maintaining a low radical concentration (i.e., radical deactivation is much faster than activation) [28]. For surface initiated ATRP with a high excess of monomer, a constant radical concentration should yield a linear relationship between mass of polymer grown from the surface and polymerization time [42,43]. And, if all of the pyridine units were accessible for ion exchange, then there would also be a linear relationship between ion-exchange capacity and polymerization time. The data, however, show a non-linear trend between the capacity and polymerization time. Since no precautions were taken to ensure controlled growth, this leveling off of capacity is likely due in part to termination or chain transfer side reactions, loss of active catalyst, or hindered mass transport of monomer to active radicals. Better control over surface-initiated polymerization can be achieved by the addition of Cu(II) to the monomer solution [42] and the use of a mixed halide initiator/catalyst system [44]. The rate of polymerization can be accelerated by increasing temperature and by using aqueous solvent conditions [45]. Furthermore, aqueous ATRP has led to thick polymer film layers [45]. Therefore, opportunities exist for increasing the degree of polymer grafting and accelerating the grafting rate, and these types of experiments are under way.

To test the functional effects of our membrane surface modification, we carried out an initial comparative study on protein adsorption. Preliminary work shows that breakthrough curves for lysozyme (feed concentration 0.02 g/L, pH 7.4) on modified PVDF membranes have a capacity at breakthrough that is 2.1 times higher than the unmodified membranes. Subsequent work is exploring the potential for using these membranes for protein separations and virus clearance and will be published at a later date.

4. Conclusions

The physical and chemical properties of commercial microporous membranes were varied by surface modification using atom transfer radical polymerization. Using this technique, membrane pore size, pore size polydispersity, and ion-exchange capacity could be adjusted using polymerization time as the independent variable. Ion-exchange capacities were low under the conditions used. However, using methods of control, as well as accelerating growth rate by changes in temperature and solvent conditions is expected to improve the degree of grafting.

By allowing the preparation of a membrane with optimized pore diameter and narrow pore size polydispersity, this approach has the potential to improve membrane efficiency by making solute retention time more uniform and sharpening solute breakthrough. Furthermore, ATRP offers flexibility to work with various chemical functionalities; as such, this technique can be used to create myriad functionalized membranes starting from a generic membrane foundation.

References

[1] J. Thömmes, M.R. Kula, Membrane chromatography—an integrative concept in the downstream processing of proteins, Biotechnol. Prog. 11 (1995) 357.

[2] D.K. Roper, E.N. Lightfoot, Separation of biomolecules using adsorptive membranes, J. Chromatogr. A 702 (1995) 3.

[3] C. Charcosset, Purification of proteins by membrane chromatography, J. Chem. Technol. Biotechnol. 71 (1998) 95.

[4] R. Giovannini, R. Freitag, T.B. Tennikova, High-performance membrane chromatography of supercoiled plasmid DNA, Anal. Chem. 70 (1998) 3348.

[5] H.N. Endres, J.A.C. Johnson, C.A. Ross, J.K. Welp, M.R. Etzel, Evaluation of an ion-exchange membrane for the purification of plasmid DNA, Biotechnol. Appl. Biochem. 37 (2003) 259.

[6] S. Brandt, R.A. Goffe, S.B. Kessler, J.L. O'Connor, S.E. Zale, Membrane-based affinity technology for commercial scale purifications, Bio/technology 6 (1988) 779.

[7] E. Klein, Affinity Membranes, Wiley, New York, 1991, pp. 131–140.

[8] M. Urnanska, P.A. Davies, M.P. Esnouf, B.J. Bellhouse, Comparative studies of reaction kinetics in membrane and agarose bead affinity systems, J. Chromatogr. 519 (1990) 53.

[9] M.A. Teeters, S.E. Conrardy, B.L. Thomas, T.W. Root, E.N. Lightfoot, Adsorptive membrane chromatography for purification of plasmid DNA, J. Chromatogr. A 989 (2003) 165.

[10] H.-C. Liu, J.R. Fried, Breakthrough of lysozyme through an affinity membrane of cellulose-cibacron blue, AIChE J. 40 (1994) 40.

[11] E. Klein, Review: affinity membranes: a 10-year review, J. Membr. Sci. 179 (2000) 1.

[12] M.M. Nasef, E.-S.A. Hegazy, Preparation and applications of ion-exchange membranes by radiation-induced graft co-polymerization of polar monomers onto non-polar films, Prog. Polym. Sci. 29 (2004) 499.

[13] M. Kim, K. Saito, S. Furusaki, T. Sugo, I. Ishigaki, Protein adsorption capacity of porous phenylalanine-containing membrane based on a polyethylene matrix, J. Chromatogr. 586 (1991) 27.

[14] M. Kim, K. Saito, S. Furusaki, T. Sato, T. Sugo, I. Ishigaki, Adsorption and elution of bovine-gamma-globulin using an affinity membrane containing hydrophobic amino acids, J. Chromatogr. 585 (1991) 45.

[15] K. Iwata, K. Saito, S. Furusaki, T. Sugo, J. Okamoto, Adsorption characteristics of an immobilized metal affinity membrane, Biotechnol. Prog. 7 (1991) 412.

[16] K. Kobayashi, S. Tsuneda, K. Saito, H. Yamagishi, S. Furusaki, T. Sugo, Preparation of microfiltration membranes containing anion-exchange groups, J. Membr. Sci. 76 (1993) 209.

[17] M. Kim, S. Kiyohara, S. Konishi, S. Tsuneda, K. Saito, T. Sugo, Ring-opening reaction of poly-GMA chain grafted onto a porous membrane, J. Membr. Sci. 117 (1996) 33.

[18] S. Kiyohara, M. Kim, Y. Toida, K. Saito, K. Sugita, T. Sugo, Selection of a precursor monomer for the introduction of affinity ligands onto a porous membrane by radiation-induced graft polymerisation, J. Chromatogr. A 758 (1997) 209.

[19] W. Guo, E. Ruckenstein, Cross-linked mercerized cellulose membranes for the affinity chromatography of papain inhibitors, J. Membr. Sci. 197 (2002) 53.

[20] W. Guo, E. Ruckenstein, A new matrix for membrane affinity chromatography and its application to the purification of concanavalin A, J. Membr. Sci. 182 (2001) 227.

[21] F. Cattoli, G.C. Sarti, Separation of MBP fusion proteins through affinity membranes, Biotechnol. Prog. 18 (2002) 94.

[22] Q. Luo, H. Zou, X. Xiao, J. Ni, High-performance affinity chromatography with immobilization of protein A and L-histidine on molded monolith, Biotechnol. Bioeng. 80 (2002) 481.

[23] E. Klein, E. Eichholz, D.H. Yeager, Affinity membranes prepared from hydrophilic coatings on microporous polysulfone hollow fibers, J. Membr. Sci. 90 (1994) 69.

[24] T.C. Beeskow, W. Kusharyoto, F.B. Anspach, K.H. Kroner, W.-D. Deckwer, Surface modification of microporous polyamide membranes with hydroxyethyl cellulose and their application as affinity membranes, J. Chromatogr. A 715 (1995) 49.

[25] M. Taniguchi, G. Belfort, Low protein fouling synthetic membranes by UV-assisted surface grafting modification: varying monomer type, J. Membr. Sci. 231 (2004) 147.

[26] J. Pieracci, J.V. Crivello, G. Belfort, Photochemical modification of 10-kDa polyethersulfone ultrafiltration membranes for reduction of biofouling, J. Membr. Sci. 156 (1999) 223.

[27] B. Yang, W.T. Yang, Photografting modification of PET nucleopore membranes, J. Macromol. Sci., Pure Appl. Chem. A40 (2003) 309.

[28] K. Matyjaszewski, J.H. Xia, Atom transfer radical polymerization, Chem. Rev. 101 (2001) 2921.

[29] X. Li, X. Wei, S.M. Husson, Thermodynamic studies on the adsorption of fibronectin adhesion-promoting peptide on nanothin films of poly(2-vinylpyridine) by SPR, Biomacromolecules 5 (2004) 869.

[30] J.D. Grandine, Making porous membranes and the membrane products, US Patent 4,203,847 (1980).

[31] K.S. Iyer, B. Zdyrko, H. Malz, J. Pionteck, I. Luzinov, Polystyrene layers grafted to macromolecular anchoring layer, Macromolecules 36 (2003) 6519.

[32] V. Klep, B. Zdyrko, Y. Liu, I. Luzinov, Polymer brushes by ATRP initiated from macroiniator synthesized on surface, in: R.C. Advincula, W.J. Brittain, K.C. Caster, J. Rühe (Eds.), Polymer Brushes: Synthesis, Characterization, Applications, Wiley–VCH Verlag, 2004.

[33] Y. Liu, V. Klep, B. Zdyrko, I. Luzinov, Polymer grafting via ATRP initiated from macroinitiator synthesized on surface, Langmuir 20 (2004) 6710.

[34] B. Zdyrko, V. Klep, I. Luzinov, Synthesis and surface morphology of high-density poly(ethylene glycol) grafted layers, Langmuir 19 (2003) 10179.

[35] T.B. Hoover, C.E. Coggan, M.S. Frant, S.R. Jenkins, F.W. Sollo, H.G. Swope, B.L. Weand, Acidity, in: A.E. Greenberg, R.R. Trussel, L.S. Clesceri, M.A.H. Franson (Eds.), Standard Methods for the Examination of Water and Wastewater, 16th ed., American Public Health Association, Washington, DC, 1985.

[36] W. Yoshida, Y. Cohen, Topological AFM characterization of graft polymerized silica membranes, J. Membr. Sci. 215 (2003) 249.

[37] V. Freger, J. Gilron, S. Belfer, TFC polyamide membranes modified by grafting of hydrophilic polymers: an FT-IR/AFM/TEM study, J. Membr. Sci. 209 (2002) 283.

[38] M. Tanaguchi, J.P. Pieracci, G. Belfort, Effect of undulations on surface energy: a quantitative assessment, Langmuir 17 (2001) 4312.

[39] K.S.W. Sing, D.H. Everett, R.A.W. Haul, L. Moscou, R.A. Pierotti, J. Rouquerol, T. Siemieniewska, Reporting physisorption data for gas/solid systems with special reference to the determination of surface area and porosity, Pure Appl. Chem. 57 (1985) 603.

[40] P.I. Ravikovitch, A.V. Niemark, Experimental confirmation of different mechanisms of evaporation from ink-bottle type pores: equilibrium, pore blocking, and cavitation, Langmuir 18 (2002) 9830.

[41] A.K. Pandey, A. Goswami, D. Sen, S. Mazumder, R.F. Childs, Formation and characterization of highly cross-linked anion-exchange membranes, J. Membr. Sci. 217 (2003) 117.

[42] K. Matyjaszewski, P.J. Miller, N. Shukla, B. Immaraporn, A. Gelman, B.B. Luokala, T.M. Siclovan, G. Kickelbick, T. Vallant, H. Hoffmann, T. Pakula, Polymers at interfaces: using atom transfer radical polymerization in the controlled growth of homopolymers and block co-polymers from silicon surfaces in the absence of untethered sacrificial initiator, Macromolecules 32 (1999) 8716.

[43] D. Gopireddy, S.M. Husson, Room temperature growth of surface-confined poly(acrylamide) from self-assembled monolayers using atom transfer radical polymerisation, Macromolecules 35 (2002) 4218.

[44] K. Matyjaszewski, D.A. Shipp, J.L. Wang, T. Grimaud, T.E. Patten, Utilizing halide exchange to improve control of atom transfer radical polymerisation, Macromolecules 31 (1998) 6836.

[45] W.X. Huang, J.B. Kim, M.L. Bruening, G.L. Baker, Functionalization of surfaces by water-accelerated atom-transfer radical polymerization of hydroxyethyl methacrylate and subsequent derivatization, Macromolecules 35 (2002) 1175.